

Theory of the microwave spectroscopy of a phosphorus-donor charge qubit in silicon: Coherent control in the Si:P quantum-computer architecture

C. J. Wellard and L. C. L. Hollenberg

Centre for Quantum Computer Technology, School of Physics, University of Melbourne, Parkville, Victoria 3010, Australia

S. Das Sarma

Condensed Matter Theory Centre, Department of Physics, University of Maryland, College Park, Maryland 20742-4111, USA

(Received 1 December 2005; revised manuscript received 22 May 2006; published 3 August 2006)

We present a theoretical analysis of a microwave spectroscopy experiment on a charge qubit defined by a P_2^+ donor pair in silicon, for which we calculate Hamiltonian parameters using the effective-mass theory of shallow donors. The master equation of the driven system in a dissipative system is solved to predict experimental outcomes. We describe how to calculate physical parameters of the system from such experimental results, including the dephasing time, T_2 , and the ratio of the resonant Rabi frequency to the relaxation rate. Finally we calculate probability distributions for experimentally relevant system parameters for a particular fabrication regime.

DOI: [10.1103/PhysRevB.74.075306](https://doi.org/10.1103/PhysRevB.74.075306)

PACS number(s): 71.55.Cn, 85.35.-p, 03.67.Lx

I. INTRODUCTION

The strong motivation supplied by the possibility of quantum information processing has recently fueled rapid progress in the experimental control of mesoscopic quantum systems. Of particular interest in the solid state are superconducting devices, and coupled quantum dots, which show promise as candidates for qubits in a scalable quantum device. In order to realize this potential it is necessary that these systems be coherently controlled with extraordinary precision, and much progress has been made toward this goal, both for superconducting systems,¹⁻³ as well as coupled quantum dots in gallium arsenide,⁴ and phosphorus doped silicon.⁵

In terms of the experimental demonstrations of coherent control, one can take two approaches. The first is the observation of Ramsey fringes in a pulsed experiment,^{1,3-5} where the coherent oscillations are between nondiagonal states of the system Hamiltonian. In such an experiment the system must be manipulated on a time scale that is fast compared to the period of the oscillations, which is the inversely proportional energy difference of the eigenstates. Alternatively one could observe the Rabi oscillations in a driven system,^{2,3} where the frequency of the oscillations is proportional to the intensity of the driving field.

In many cases a precursor to these achievements is the somewhat simpler procedure of performing a spectroscopic measurement of the device.⁶⁻⁸ This is achieved by driving the system of interest at particular frequency, and varying parameters to bring the system into resonance. When in resonance, the system will undergo Rabi oscillations, however a spectroscopic experiment of this nature does not resolve these oscillations, instead measurements are made on a time scale that is greater than the Rabi frequency, giving a time averaged result. Useful results can be obtained even in the regime in which the frequency of the oscillation is slow compared with relevant decoherence times. Clearly a measurement of this type places far fewer demands on the system

than if the fringes are to be resolved, however, useful information can still be obtained, such as the dephasing time T_2 , some of the system energy scales, and the ratio of the resonant Rabi frequency to the relaxation rate.

One of the most promising quantum computer architectures, particularly from the all-important scalability perspective, is the phosphorus-doped silicon (Si:P) system, where the shallow P-bound electronic donor states are electrically manipulated by external gates for the quantum control of the qubits. In spite of impressive recent growth, fabrication, and theoretical developments in the Si:P quantum computer architecture, the key ingredient of an experimental demonstration of coherent quantum dynamics at the single qubit level is still lacking. In this paper we consider a specific experimental setup, namely the externally driven microwave spectroscopy of a P_2^+ charge qubit⁹ (i.e., the singly ionized coupled P-P effective “molecular” system in Si with two nearby ion implanted P atoms sharing one electron), giving a detailed quantitative theoretical analysis to establish the feasibility of this coherent single qubit control experiment in currently available Si:P devices. We believe that the qubit coherent control experiment proposed and analyzed in this work may very well be the simplest single qubit measurement one could envision in the (Si:P) quantum computer architecture, and as such, our detailed quantitative analysis should motivate serious experimental efforts using microwave spectroscopy.

Such an experiment is a necessary prerequisite for further experimental progress in coherent qubit control and manipulation in the Si:P quantum computer architecture. Our detailed theory provides the quantitative constraints on the experimental system parameters required for developing the coherent control of the Si:P system, and in addition, establishes how one can extract important decoherence parameters (e.g., T_2) from the experimental data. A knowledge of charge coherence times for phosphorus-in-silicon structures is important, not just for charge-based quantum information pro-

cessing, but also for spin based proposals as charge fluctuations can lead directly to dephasing of exchange coupled spin qubits.¹⁰ Additionally, most spin readout proposals involve a spin-to-charge conversion,^{11–13} and several proposals call for the electron spin to be transported around the device, to interact with non-neighboring qubits.^{14,15} Both of these processes will ultimately be limited by the charge coherence time.

The energetics of this P_2^+ system, including its interaction with phonon modes in the lattice,¹⁶ and with a dc electric field,¹⁷ have been studied by previous authors, while a theoretical investigation of the microwave spectroscopy of a coupled quantum dot in a GaAs system has been carried out by Barrett and Stace,¹⁸ and much work has been done on the theory of the dynamics of driven systems coupled to dissipative environments and has been well studied in the context of flux qubits.^{19,20}

In this paper we begin by reviewing the P_2^+ in the silicon system in the presence of an electric field, and outline the calculation of the Hamiltonian matrix elements for use in the calculation of the system dynamics. In Sec. III we derive a master equation for the driven system, in the presence of three decoherence channels, following the approach of Ref. 18. This master equation is analytically solved for the steady-state solutions, valid on a time scale that is long compared to the relaxation time. To probe the dynamics on shorter time scales requires, in general, numerical integration of the master equation. In Sec. IV we show how it is possible to use the output of the measurement device to obtain the energy scales of the system, and to calculate the dephasing time T_2 . In Sec. V we briefly discuss possibilities for the direct observation of coherent oscillations in this system. Finally, in Sec. VI, we discuss the statistical nature of the device fabrication, calculate probability distributions for experimentally relevant parameters, and discuss their effects on experimental outcomes.

II. A TWO-DONOR CHARGE QUBIT IN SILICON

We consider a system defined by the electronic state of a pair of phosphorus donors in silicon, which has been singly ionized such that the system has a single net positive charge,⁹ as illustrated in Fig. 1. The donor nuclei are separated by a vector \mathbf{R} , and in the absence of externally applied fields, the system Hamiltonian is

$$H_0(\mathbf{r}) = H_{\text{Si}}(\mathbf{r}) + V_d(\mathbf{r} - \mathbf{R}/2) + V_d(\mathbf{r} + \mathbf{R}/2). \quad (1)$$

Here H_{Si} is the Hamiltonian of an electron in the pure silicon lattice, which includes both a kinetic term and the effective potential due to the silicon lattice. Solutions of this silicon Hamiltonian are the Bloch functions of the pure silicon crystal. The $V_d(\mathbf{r})$ terms give the impurity potential of the ionic donor cores, which we will treat as Coulombic, $V_d(\mathbf{r}) = -2/(\kappa r)$, with $\kappa = 11.9$, the dielectric constant of silicon.

The electronic ground state for a single donor, centered at a position $\mathbf{R}/2$, is, in the effective-mass approximation, given by the Kohn-Luttinger wave function,²¹

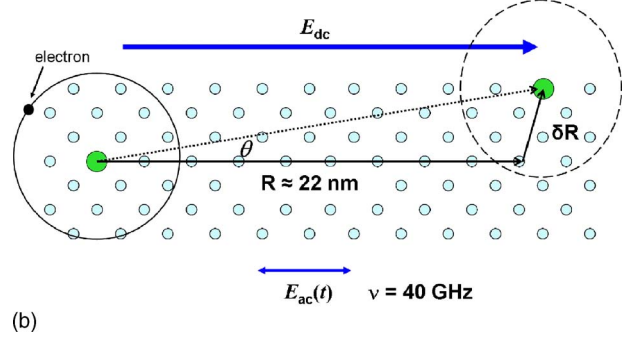
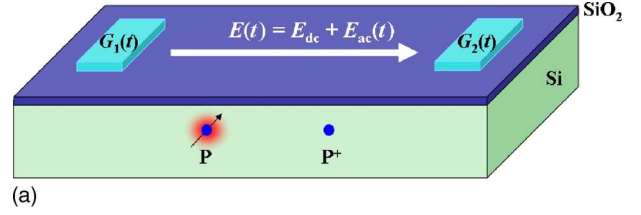


FIG. 1. (Color online) On the top is a schematic of the experimental setup showing the location of the bias gates relative to the phosphorus donors. On the bottom is a diagram showing orientation of the two donors, and the direction of the applied fields, relative to the silicon crystal lattice.

$$\psi(\mathbf{r}) = \sum_{\mu} F_{\mu}(\mathbf{r} - \mathbf{R}/2) u_{\mathbf{k}_{\mu}}(\mathbf{r}) e^{i\mathbf{k}_{\mu}(\mathbf{r} - \mathbf{R}/2)}. \quad (2)$$

In this equation the sum is over the six degenerate minima of the silicon conduction band, \mathbf{k}_{μ} denoting the reciprocal lattice vector at the minima μ . The function $u_{\mathbf{k}_{\mu}}(\mathbf{r})$ is the periodic part of the conduction band Bloch function, and $F_{\mu}(\mathbf{r})$ is a nonisotropic, hydrogenlike envelope function, which for the $\pm z$ minima takes the form

$$F_{\pm z} = \frac{e^{-\sqrt{z^2/a_{\parallel}^2 + (x^2 + y^2)/a_{\perp}^2}}}{\sqrt{6\pi a_{\perp}^2 a_{\parallel}}}, \quad (3)$$

where a_{\parallel}, a_{\perp} are the nonisotropic effective Bohr radii resulting from the anisotropy of the conduction band minima. In the presence of an applied field, such as those considered in this work, the T_d symmetry of the Hamiltonian is broken. This can lead to a ground state with unequal contributions from Bloch functions at the six conduction band minima, however this effect is small at the field strengths considered.²³

A full treatment of the two-donor system would include an *ab initio* analysis of the molecular states of the system, however, if R is sufficiently large, the low-lying energy states of the two-center system are approximated by even and odd superpositions of the single donor ground states,

$$\Psi_{\pm}(\mathbf{r}) = [\psi(\mathbf{r} - \mathbf{R}/2) \pm \psi(\mathbf{r} + \mathbf{R}/2)] / \sqrt{2(1 \pm S^2)},$$

with $S = \int \psi^*(\mathbf{r} - \mathbf{R}/2) \psi(\mathbf{r} + \mathbf{R}/2) d\mathbf{r}$. Interference between the Bloch functions associated with the different conduction-band minima leads to a nonmonotonic dependence of the symmetric-antisymmetric energy gap, Δ_{s-as} , on the magni-

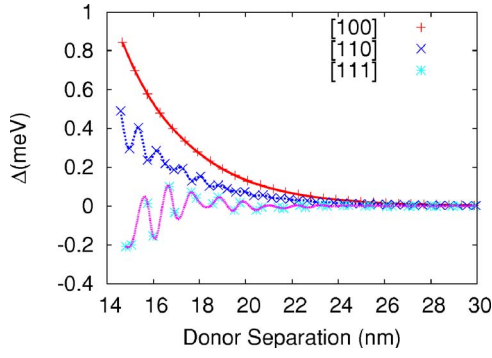


FIG. 2. (Color online) A plot of the symmetric-antisymmetric energy gap Δ_{s-as} , as a function of donor separation along three high symmetry crystallographic axes. The points denote fcc lattice sites, the lines are a guide to the eye.

tude separation of the donors, as well as on their orientation with respect to the silicon substrate.¹⁶ This is illustrated in Fig. 2, where we plot Δ_{s-as} as a function of donor separation, for donors separated along three high symmetry crystallographic axes, note that for certain separations the ground state is actually the antisymmetric state. The intervalley interference is less pronounced for donors separated along a [100] axis, where the energy splitting can be well approximated by a hydrogenic expression,²² with an effective Bohr radius $a_B^* \approx 2.5$ nm. For donors not separated along the [100] axis, including those separated along other high symmetry axes such as the [111], interference effects dominate, and the energy splitting defies description using a hydrogenic model.

The Hamiltonian matrix, in the basis of single donor ground states, $\{|L\rangle, |R\rangle\}$, is determined by numerical integration, and can be parametrized as

$$H_0 = h_x \sigma^x + h_z \sigma^z, \quad (4)$$

where the coefficients are given by $h_z = (\langle L|H_0|L\rangle - \langle R|H_0|R\rangle)/2$ and, $h_x = \langle L|H_0|R\rangle$. Note that we have ignored the constant term, and defined our basis of states such that the σ^y component is zero. In practice we expect that the two donors are identical, in which case $h_z = 0$, however we retain this term in what follows for generality.

Throughout this paper we will consider the application of uniform electric fields, both ac and dc, which are applied along a crystallographic [100] axis. This is not, in general, parallel to the donor separation \mathbf{R} , which we allow to vary. The addition of such a field, \mathbf{E} , gives rise to a potential $V(\mathbf{r}) = -e \mathbf{E} \cdot \mathbf{r}$, the potential matrix in the $\{|L\rangle, |R\rangle\}$ basis is calculated by numerical integration, and can be written as

$$V_{ac,dc} = E_{ac,dc} (\xi_x \sigma^x + \xi_z \sigma^z), \quad (5)$$

with

$$\xi_z = (\langle L|V|L\rangle - \langle R|V|R\rangle)/(2E_{ac,dc}),$$

and

$$\xi_x = \langle L|V|R\rangle/E_{ac,dc}.$$

In the case of radially symmetric single donor wave functions, the ξ_x term is identically zero, however this symmetry

is broken by the silicon lattice. In practice we find $\xi_z \gg \xi_x$, where the magnitude of this difference is dependent on \mathbf{R} . For donor spacings of the order $R \approx 20$ nm, we find $\xi_z/\xi_x \sim 100-1000$.

To begin with, we consider the effect of a dc field,

$$H = H_0 + V_{dc} = (h_x + E_{dc}\xi_x)\sigma^x + (h_z + E_{dc}\xi_z)\sigma^z = \Theta \sigma^z e^{i\phi\sigma^y}. \quad (6)$$

Here $\Theta = \sqrt{(h_x + E_{dc}\xi_x)^2 + (h_z + E_{dc}\xi_z)^2}$, and $\phi = \arctan[(h_x + E_{dc}\xi_x)/(h_z + E_{dc}\xi_z)]$. Thus, the above Hamiltonian can be diagonalized via the transformation

$$H' = U_1 H U_1^\dagger = \Theta \sigma^z, \quad (7)$$

with $U_1 = \exp(i\phi\sigma^y/2)$. The eigenvalues are given by $\lambda_{\pm} = \pm\Theta$, and the eigenstates, in the original charge localized basis, by

$$\begin{aligned} |+\rangle &= \cos(\phi/2)|L\rangle - \sin(\phi/2)|R\rangle, \\ |-\rangle &= \sin(\phi/2)|L\rangle + \cos(\phi/2)|R\rangle. \end{aligned} \quad (8)$$

Thus, by varying the strength of the dc field, we can alter the energy splitting between the two lowest energy states, $\Delta = 2\Theta$, as well as the degree of localization of the eigenstates $\chi_{\pm} = |\langle L|\pm\rangle|^2 = [1 \pm \cos(\phi)]/2$.

The addition of an ac field of angular frequency ω applied in the same direction as the uniform dc field adds a term to the Hamiltonian

$$V_{ac} = E_{ac} \cos(\omega t) (\xi_x \sigma^x + \xi_z \sigma^z). \quad (9)$$

This transforms to the eigenbasis of the time-independent system as

$$V'_{ac} = U_1 V_{ac} U_1^\dagger = E_{ac} \cos(\omega t) (\sigma^x \gamma_x + \sigma^z \gamma_z), \quad (10)$$

with $\gamma_x = \xi_x \cos(\phi) - \xi_z \sin(\phi)$, $\gamma_z = \xi_z \cos(\phi) + \xi_x \sin(\phi)$.

We now transform into an interaction picture, rotating at the same frequency as the ac field. The transformation is defined by $U_2(t) = \exp(i\omega t \sigma^z/2)$. Evolution in this frame is generated by the Hamiltonian

$$\tilde{H}' = \left(\Theta - \frac{\omega}{2} \right) \sigma^z + E_{ac} \cos(\omega t) (\sigma^x \gamma_x e^{-i\omega t \sigma^z} + \sigma^z \gamma_z). \quad (11)$$

It is at this point that it becomes convenient to make a rotating wave approximation (RWA), in which we ignore terms that are rotating with frequency ω . This approximation is valid if $\omega \gg E_{ac} \gamma_x, E_{ac} \gamma_z$, and reduces the above Hamiltonian to

$$\tilde{H}' = \left(\Theta - \frac{\omega}{2} \right) \sigma^z + E_{ac} \frac{\gamma_x}{2} \sigma^x. \quad (12)$$

III. CONSTRUCTION OF THE MASTER EQUATION

To describe the effects of a dissipative environment on the dynamics of the system, it is necessary to construct a master equation. We consider the effects of three channels of deco-

herence, namely, dephasing, relaxation, and excitation, with different rates Γ_z , Γ_- , Γ_+ , respectively. We expect these channels to be sufficient to describe most physical noise sources,^{24,25} including interaction with the measurement device.^{18,26,27} Generally we would expect Γ_z to be the dominant term, with the relaxation term $\Gamma_- < \Gamma_z$. The excitation term is included for generality, and allows the description of the effects of classical, or high temperature noise sources, we expect $\Gamma_+ \leq \Gamma_-$.

In the rotating frame, the master equation is given by

$$\begin{aligned} \dot{\tilde{\rho}}'(t) = & -i \left[\left(\Theta - \frac{\omega}{2} \right) \sigma^z + E_{ac} \frac{\gamma_x}{2} \sigma^x, \tilde{\rho}'(t) \right] + \Gamma_z \mathcal{L}\{\sigma^z, \tilde{\rho}'(t)\} \\ & + \Gamma_- \mathcal{L}\{\sigma^-, \tilde{\rho}'(t)\} + \Gamma_+ \mathcal{L}\{\sigma^+, \tilde{\rho}'(t)\}, \end{aligned} \quad (13)$$

with the Lindblad terms $\mathcal{L}\{L_i, \rho\} = L_i \rho L_i^\dagger - (L_i^\dagger L_i \rho + \rho L_i^\dagger L_i)/2$.

The steady state solution of this master equation gives the asymptotic form for the components of the polarization vector, defined by $\rho = (I + X\sigma^x + Y\sigma^y + Z\sigma^z)/2$. In the rotating frame these are

$$\begin{aligned} \tilde{X}'(\infty) &= \frac{-8\eta E_{ac} \gamma_x (\Gamma_+ - \Gamma_-)}{16(\Gamma_+ + \Gamma_-) \eta^2 + [2(E_{ac} \gamma_x)^2 + (\Gamma_+ + \Gamma_-)(\Gamma_+ + \Gamma_- + 4\Gamma_z)](\Gamma_+ + \Gamma_- + 4\Gamma_z)}, \\ \tilde{Y}'(\infty) &= \frac{2\eta E_{ac} \gamma_x (\Gamma_+ - \Gamma_-)(\Gamma_+ + \Gamma_- + 4\Gamma_z)}{16(\Gamma_+ + \Gamma_-) \eta^2 + [2(E_{ac} \gamma_x)^2 + (\Gamma_+ + \Gamma_-)(\Gamma_+ + \Gamma_- + 4\Gamma_z)](\Gamma_+ + \Gamma_- + 4\Gamma_z)}, \\ \tilde{Z}'(\infty) &= (\Gamma_+ - \Gamma_-) \frac{16\eta^2 + (\Gamma_+ + \Gamma_- + 4\Gamma_z)^2}{16\eta^2(\Gamma_+ + \Gamma_-) + [2(E_{ac} \gamma_x)^2 + (\Gamma_+ + \Gamma_-)(\Gamma_+ + \Gamma_- + 4\Gamma_z)](\Gamma_+ + \Gamma_- + 4\Gamma_z)}, \end{aligned} \quad (14)$$

where $\eta = \Theta - \omega/2$ is the detuning of the microwave field.

We wish to calculate the expected output from a detector which measures charge localization, a z measurement in the original basis, and therefore are interested in calculating the Z component of the polarization vector in the charge localized basis and the laboratory frame, the asymptotic form of which is given by

$$Z(t) = \tilde{Z}'(\infty) \cos(\phi) - [\cos(\omega t) \tilde{X}'(\infty) + \sin(\omega t) \tilde{Y}'(\infty)] \sin(\phi). \quad (15)$$

In the case that the measurement time of the detector is long compared to both the relaxation time scale, $t_{\text{det}} > 1/\Gamma_-$, and the time scale of these oscillations $t_{\text{det}} > 1/\Omega$, the system reaches the steady state equilibrium over the time of the measurement, and the rapid oscillations of the rotating frame will average out. In this case the probability of measuring the electron to be localized at the position of the left donor is given by $P_L = [1 + \cos(\phi) \tilde{Z}'(\infty)]/2$.

IV. APPLICATION

We now turn our attention to analysis of simulated experimental results. In practice the P-P⁺ charge qubit is, in the first instance, fabricated via ion implantation,²⁸ whereby 14 keV phosphorus ions are implanted into a silicon crystal. Such a process is imprecise and there will be significant uncertainty in the position of the two phosphorus donors. As we have previously discussed, this will be manifest in an uncertainty in both the bare Hamiltonian of the two donor system, as well as in the potential arising from the applied electric fields. To illustrate how this uncertainty will affect experi-

mental results, we have calculated simulated experimental traces P_L as a function of applied dc field E_{dc} , for donor pairs with slightly varying separations, using driving field of frequency 40 GHz and amplitude $E_{ac} = 10^{-2}$ MV m⁻¹. The results are plotted in Fig. 3, and show that although a slight variation of the donor separation has little effect on the position of the resonance peak, both the width and height of the peak are strongly affected.

In addition to the system Hamiltonian parameters, an experimental trace will be effected by the strength of the decoherence channels, as shown in Fig. 4. Here we see that both the height and the width of the peaks are dependent of the

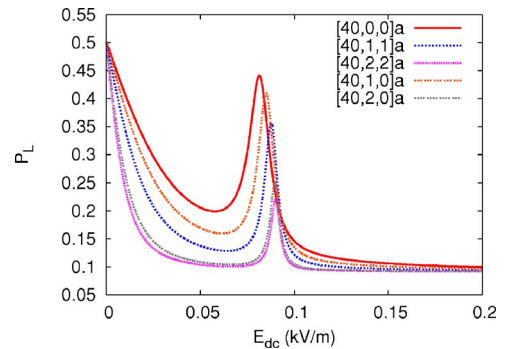


FIG. 3. (Color online) Donor spectroscopy for several donor separations with a small deviation from the ideal separation of $R = [40a, 0, 0]$, where $a = 0.543$ nm is the lattice constant of silicon. The data show that the peak heights and positions are not strongly dependent on these positional variations, however the width of the peak changes significantly. All data were calculated with a 40 GHz driving field of amplitude $E_{ac} = 10^{-2}$ MV/m, and decoherence rates $\Gamma_z = 3$ GHz, $\Gamma_- = 1$ GHz, and $\Gamma_+ = 100$ MHz.

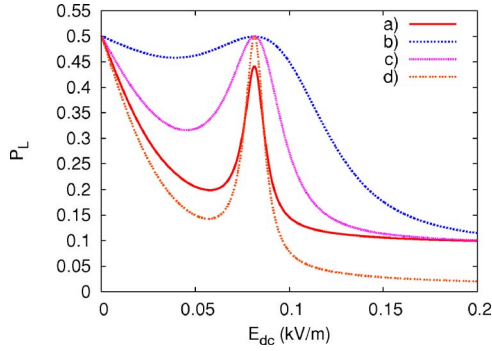


FIG. 4. (Color online) An illustration of the effects of various decoherence channels on the spectroscopic signal height. These channels affect both the peak height and width as described in the text. The lengths are in units of $a=0.543$ nm, the lattice constant of silicon all data in this plot were taken for a donor separation $R=[40a,0,0]$, where $a=0.543$ nm is the lattice constant of silicon. The frequency of the driving field was 40 GHz and its amplitude $E_{ac}=0.01$ MV m $^{-1}$. The decoherence rates are (a) $\Gamma_z=3$ GHz, $\Gamma_- = 1$ GHz, $\Gamma_+ = 100$ MHz, (b) $\Gamma_z=3$ GHz, $\Gamma_- = 10$ MHz, $\Gamma_+ = 1$ MHz, (c) $\Gamma_z=300$ MHz, $\Gamma_- = 10$ MHz, $\Gamma_+ = 1$ MHz, (d) $\Gamma_z = 300$ MHz, $\Gamma_- = 100$ MHz, $\Gamma_+ = 1$ MHz.

rates of decoherence, while the position of the peak is determined by the eigenenergies of the system. It is, therefore, reasonable to expect that useful information about the system can be obtained from the analysis of these spectroscopic data.

Given an experimental trace, we would like to determine useful spectroscopic information about the qubit, in particular we would like to determine decoherence times, as well as the energy scales of the system. Here we assume that the detector signal is proportional to the quantity P_L , however the constant of proportionality may not be known. A way of determining this is to consider the signal in the absence of the ac field, where $P_L=[1+(\Gamma_+-\Gamma_-)\cos(\phi)]/(\Gamma_++\Gamma_-)]/2$. Taking the ratio of the signal values at large positive and negative values of the dc field, where $\cos(\phi)=\pm 1$ depending on the polarity of the field, gives the value of Γ_+/Γ_- , this allows the constant of proportionality to be determined. With this information it is possible to evaluate $\cos(\phi)$ over a range of values of E_{dc} , by observation of the detector signal as a function of the dc field.

In general, the strength of the applied electric fields, both ac and dc, at the position of the qubit, may not be known for a given control gate bias. In what follows we will assume that both these quantities are linear functions of their respective voltage biases, $E_{dc}=\alpha G_{dc}$, $E_{ac}=\beta G_{ac}$ where the G_{dc}, G_{ac} are known experimental control parameters.

By obtaining several traces taken at different driving frequencies, and observing the positions of the resonance peaks E_{dc}^* , it is possible to obtain values for Θ as a function of G_{dc} . Combined with the knowledge of $\cos \phi$, this allows us to obtain values for $\alpha\xi_z$ and h_x .

Additional information can be gained from measuring the width of the resonance peak, the half-width at half-maximum, measured from the flat baseline value, is given by the expression

$$\Delta G_{dc} = \frac{1}{2\alpha\xi_z} \sqrt{\frac{[2(E_{ac}\gamma_x)^2 + (\Gamma_+ + \Gamma_-)(\Gamma_+ + \Gamma_- + 4\Gamma_z)](\Gamma_+ + \Gamma_- + 4\Gamma_z)}{\Gamma_+ + \Gamma_-}}. \quad (16)$$

Here we have assumed that $\cos(\phi)=1$ at the position of the resonance, which is a good approximation in most cases, as shown in Fig.6(d). If this is not the case, a slightly more complicated expression can be derived for Eq. (16). If traces can be evaluated for different values of the microwave power, the above expression gives information about the decoherence rates, in particular extrapolation to zero microwave power yields $\Delta G_{dc}=(\Gamma_++\Gamma_-+4\Gamma_z)/(2\alpha\xi_z)$. Given that $\alpha\xi_z$ has already been determined, this allows direct evaluation of the dephasing time $T_2=4/(\Gamma_++\Gamma_-+4\Gamma_z)$. Another useful expression is that for the height of the resonance peak,

$$h \approx \frac{1}{2} \left(1 + \frac{(\Gamma_+ - \Gamma_-)(\Gamma_+ + \Gamma_- + 4\Gamma_z)}{2(E_{ac}\gamma_x)^2 + (\Gamma_+ + \Gamma_-)(\Gamma_+ + \Gamma_- + 4\Gamma_z)} \right), \quad (17)$$

where we have again assumed $\cos(\phi)=1$ at resonance.

V. MEASUREMENT OF COHERENT OSCILLATIONS

A somewhat more demanding experiment would be to attempt to resolve coherent oscillations of the system. This can be done with either Rabi oscillations² or Ramsey oscillations.^{1,4,5} Rabi oscillations are resonant driven oscillations of the type described in this paper, where the Rabi frequency is given by $E_{ac}\gamma_x$. In order to be able to observe Rabi oscillations, it is necessary that the oscillation period be long compared to the time resolution of the detector $t_{det} < 1/(E_{ac}\gamma_x)$, or alternatively, that the state can be shelved for measurement. In either case, the Rabi frequency must be fast compared to the dephasing time $E_{ac}\gamma_x > \Gamma_z + \Gamma_+ + \Gamma_-$. We have calculated a distribution of Rabi frequencies, in units of the applied ac field strength, for a certain fabrication strategy that is described in the following section, and plotted the results in Fig. 6(e). From this we can see that for an ac field strength of $E_{ac}=0.01$ MV m $^{-1}$, the value used for all calculations in this paper, and one which is possibly at the high end of what could be reasonably expected to be experimen-

tally generated, the Rabi frequency is almost certain to be significantly less than 500 MHz. This is likely to be slow compared to realistic dephasing rates, making resolution of Rabi oscillations unlikely.

For most quantum systems, and this case is no different, it may be more practical to attempt to measure the Ramsey oscillations. These are the coherent oscillation between basis states that are not eigenstates of the system Hamiltonian. The advantage observing Ramsey oscillation over Rabi oscillation is that the frequency of the Ramsey oscillations is significantly higher than the typical Rabi frequency. The frequency of the Ramsey fringes is given by the energy difference between eigenstates, 2Θ , and can be increased with the application of a dc field E_{dc} , to at least 40 GHz. Apart from the obvious condition $2\Theta > \Gamma_z + \Gamma_+ + \Gamma_-$, and assuming that the system can be shelved for measurement, the experimental requirements for resolution of these oscillations are that the measurement time is fast compared to the relaxation time $t_{det} < 1/\Gamma_-$, and that the system can be manipulated on a time scale that is fast compared to the period of oscillations.

In general, Ramsey oscillations are significantly easier to observe than Rabi oscillation, and have been observed in both superconducting systems,^{1,3} as well as coupled quantum dots,⁴ while Rabi oscillations have been resolved in superconducting systems,^{2,3} but not in coupled quantum dots.

VI. UNCERTAINTIES DUE TO IMPRECISE FABRICATION

We now turn our attention to uncertainties that may arise due to the statistical nature of the fabrication procedure for such a device. In the long term, the most precise way of fabricating a gated P-P⁺ device, such as those considered in this paper, is via the atomically precise placement of phosphorus donors in a silicon substrate using STM based hydrogen lithography techniques,²⁹ however this is presently beyond the current capabilities of the technique. At present, the only practical way to create such a device is via the ion implantation of a pair of phosphorus donors.²⁸ Interactions of the ions with the host silicon atoms during implantation give rise to a phenomenon known as straggle, which results in an uncertainty in the final position of the donors. Implantation of 14 keV phosphorus ions in silicon results in a roughly Gaussian donor distribution, centered approximately 20 nm below the silicon surface, and with a deviation $\sigma \approx 10$ nm. In addition to this ion straggle, is an uncertainty in where the ion strikes the substrate, due to the ion beam spot size. Current fabrication techniques involve implanting into a 30 nm aperture, with the ion distribution over this aperture roughly uniform.

In this section we analyze several different implantation strategies, and discuss which is most likely to yield a donor pair for which a spectroscopic measurement can be made. This involves maximizing the strength of the Rabi frequency of the system, which is given by the expression $\gamma_x \sim \xi_x \sin(\phi)$. The parameter ξ_x increases linearly with donor separation, but decreases as the component of the field in the direction of the donor separation decreases. We thus expect

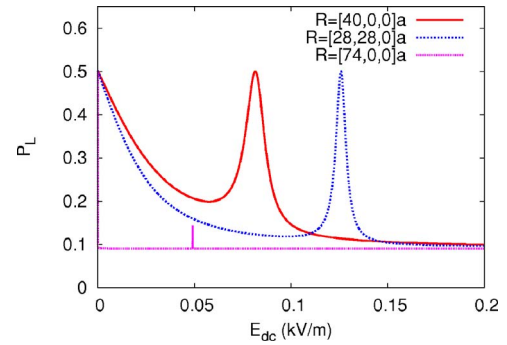


FIG. 5. (Color online) Donor spectroscopy for sample traces for donors of significantly different separations. This data plot is intended to illustrate that increasing the angle between the donor separation and the direction of the applied fields has less effect on the spectroscopic system than increasing the donor separation. All data were calculated with a 40 GHz driving field of amplitude $E_{ac} = 10^{-2}$ MV/m, and decoherence rates $\Gamma_z = 30$ MHz, $\Gamma_- = 10$ MHz, and $\Gamma_+ = 1$ MHz.

this parameter to be maximized in the two aperture fabrication scheme. Competing with this however is the $\sin(\phi)$ term, which decreases exponentially with donor separation. It thus seems reasonable that taking the approach of reducing the expected donor separation will produce the best devices. This point is illustrated in Fig. 5, where we have plotted simulated detector outputs for three scenarios, one in which the donors are separated by approximately $R = 22$ nm, in the [100] direction, parallel to the field. The donors are separated by the same distance in the second trace, but have been rotated by 45 degrees with respect to the field. The plot shows that this has little effect on the shape of the peak, however the location of the peak has been shifted to higher fields, reflecting the reduced component of the field in the direction of the donor separation. Finally the third trace has been calculated for donors separated by $R = 40$ nm, this peak is barely discernible.

One strategy involves implanting single ions into two separate apertures, with the centers of the apertures aligned along the direction of the applied electric field. This strategy maximizes the expected component of the field along the axis of the donor separation, but means that the expected donor separation will be large. A second strategy is to implant both donors into the same aperture, decreasing the expected donor separation, but increasing the probability that the donors are aligned perpendicular to the applied electric field. Finally we consider the effect of implanting a single P₂ molecular ion at 28 meV, this would decrease the expected donor separation even further.

To compare these strategies we have calculated the distributions of key system parameters that would be expected from the different approach. This was done using an ensemble of 26 000 points from a distribution appropriate to the particular strategy. The ion straggle was assumed to give a Gaussian distribution with a variation $\sigma = 10$ nm, and this was convoluted with the aperture function, with the distribution over each aperture assumed to be uniform. In the case of the P₂ implant no aperture function was required, as both donors are guaranteed to enter the substrate at the same

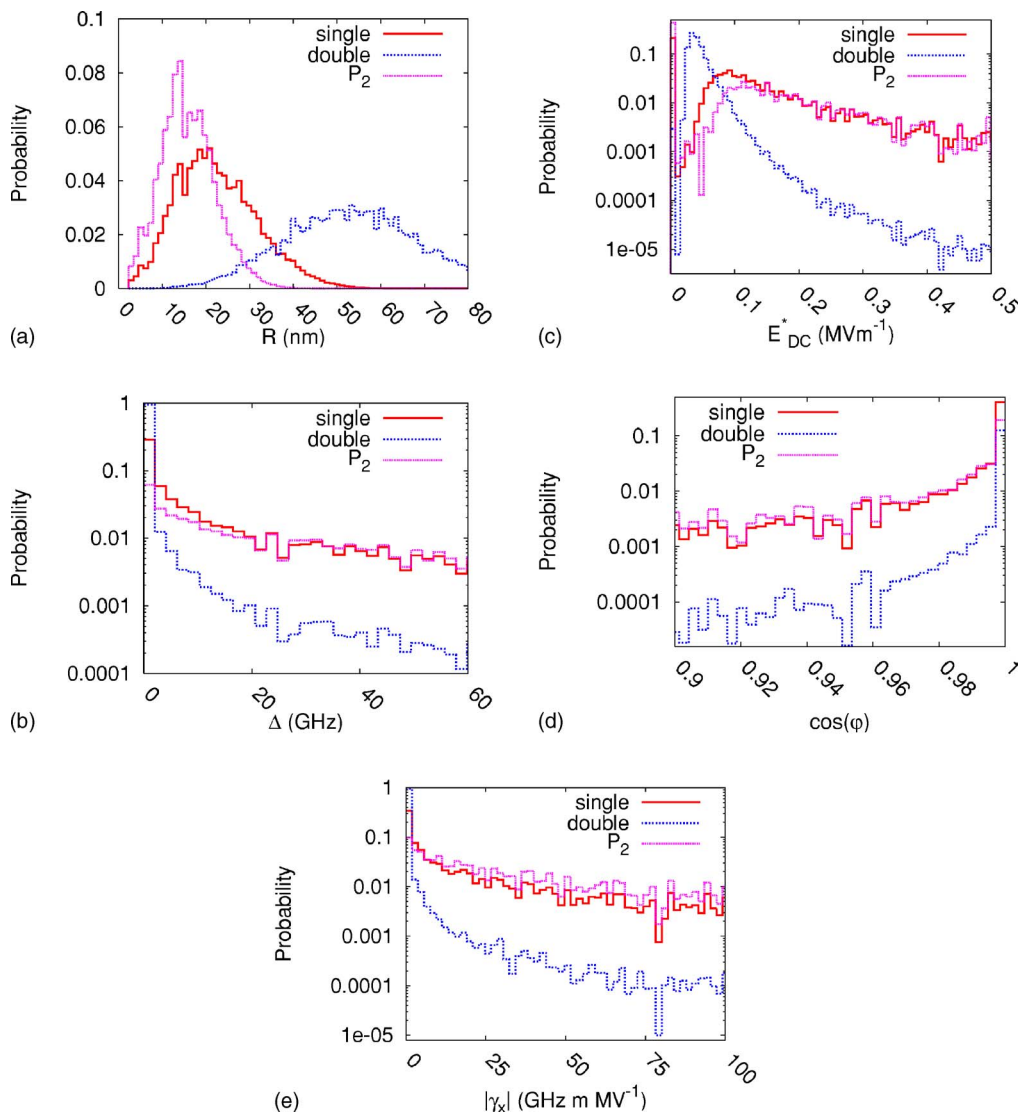


FIG. 6. (Color online) Probability distributions of system parameters for several donor implantation strategies. The first, labeled single, involves the 14 keV implantation of two single phosphorus ions in a single aperture of side length 30 nm. The second strategy, labeled double, involves a 14 keV implant of one atom in each of two similar apertures, centered at a distance 50 nm apart along a 100 axis. The final strategy involves the 28 keV implantation of a single P_2 molecule in a single aperture. These data were obtained using an ensemble of 27 000 randomly chosen points. (a) The distribution of donor separations R . (b) A log-scale plot of the distribution of the energy gap between the ground and first-excited states of the unperturbed qubit, Δ . (c) A log-scale plot of the distribution of the dc field strength required to bring the system into resonance with a 40 GHz field. (d) A log-scale plot of the distribution of ϕ , the angle that parametrizes the degree of localization of the ground state. (e) A log-scale plot of the distribution of the magnitude of γ_x , the resonant Rabi frequency.

point. The results for each of the three implantation strategies are plotted in Fig. 6.

The distribution of the magnitude of the donor separation is shown in Fig. 6(a), which shows that the expected donor separation is significantly larger for the two aperture strategy, while the P_2 implant reduces the expected separation. The distribution of the unperturbed energy gap, Δ , is plotted on a log scale in Fig. 6(b). This is the magnitude of the value Δ_{s-as} discussed in Ref. 16, for the purposes of a microwave spectroscopy experiment the sign of this quantity is unimportant. As expected, this quantity is more strongly peaked at low frequencies for the double aperture implant, and this strategy gives a much lower probability of producing $\Delta > 40$ GHz, which would make observation of a single photon resonance

peak using 40 GHz microwave radiation impossible. Although two-photon resonances may still be observed, they will be of significantly diminished magnitude, to get an observable signal from these samples it would be necessary to use higher frequency microwaves. A log-scale plot of the distributions of the dc field required to bring the system into resonance, E_{dc}^* , is presented in Fig. 6(c). In this plot the peaks at zero field represent the probability that $\Delta > 40$ GHz, in which case the system cannot be brought into resonance with the microwave field at any value of E_{dc} . The double aperture distribution is far more strongly skewed at low biases, reflecting the increased donor separation and the better alignment with the applied field that is a consequence of that separation. Figure 6(d) shows a log-scale plot of the distri-

bution of the quantity $\cos(\phi)$ at resonance. This angle reflects the degree to which the system eigenstates are given by the charge localized states, as expressed in Eq. (8). The fact that this distribution is strongly peaked around 1 indicates that at resonance the eigenstates are likely to be the charge localized states, and that the approximation made in deriving expression (16) is likely to be well satisfied. Finally, Fig. 6(e) shows a log-scale plot of the distribution of the magnitude of the Rabi frequencies, in units of the applied ac field strengths. Here we see that the single aperture implantation strategy offers a much higher probability of producing an observable Rabi frequency than does the two aperture implantation strategy, and the P_2 implantation strategy offers an improvement on the single aperture, two ion implantation.

It is this Rabi frequency that is the most important parameter, the higher the Rabi frequency, the more likely that the resonance peak can be observed. From the above data, it is clear that implanting in two well separated apertures is unlikely to produce an observable signal. Implanting in a single aperture, while producing a significant probability that the unbiased energy splitting Δ is too large for the system to be driven by a 40 GHz field, none the less, increases the probability of producing an observable signal significantly. Implanting with a 28 keV P_2 ion, increases this chance even more, due to the reduced donor separation.

VII. CONCLUSION

We have developed in this paper a detailed quantitative theory for the electric field tuned microwave spectroscopic coherent response of the electronic P_2^+ charge qubits in silicon. Our realistic calculation, taking into account fabrication

and ion implantation aspects of the sample preparation, shows convincingly that such an electric field tuned coherent microwave response measurement to be feasible in the P_2^+ donor qubit system. In addition, we establish that such a measurement would directly provide information on the characteristic decoherence and visibility times for P_2^+ charge qubits. We find that the “exchange-oscillation” type quantum interference problem,³⁰ arising from the six-valley degeneracy in the Si conduction band, does not lead to any specific difficulties in the interpretation of the microwave spectroscopy proposed herein. Our proposed microwave experiment along with the recent dc experiment proposed by Koiller *et al.*,¹⁷ which complements our proposal, are essential prerequisites for the eventual observation of Rabi and Ramsey coherent oscillations in the Si quantum computer architecture.

Finally we analyze several ion-implantation strategies for fabrication of such a device. We conclude that a single aperture implant strategy offers a far better opportunity for producing an observable Rabi frequency, and that implanting with a single P_2 ion increases this likelihood further.

ACKNOWLEDGMENTS

Two of the authors (C.W. and L.H.) acknowledge financial support from the Australian Research Council, the Australian Government and by the U.S. National Security Agency (NSA), Advanced Research and Development Activity (ARDA), and the Army Research Office (ARO) under Contract No. DAAD19-01-1-0653. One of the authors (S.D.S.) is supported by the LPS-NSA and the ARO. One of the authors (C.W.) would also like to acknowledge discussions with S. Barrett.

-
- ¹Y. Nakamura, Y. A. Pashkin, and J. S. Tsai, *Nature (London)* **398**, 786 (1999).
²Y. Nakamura, Y. A. Pashkin, and J. S. Tsai, *Phys. Rev. Lett.* **87**, 246601 (2001).
³D. Vion, A. Aouine, A. Cottet, P. Joyez, H. Pothier, C. Urbina, D. Esteve, and M. Devoret, *Fortschr. Phys.* **51**, 462 (2003).
⁴T. Hayashi, T. Fujisawa, H. D. Cheong, Y. Jeong, and Y. Hirayama, *Phys. Rev. Lett.* **91**, 226804 (2003).
⁵J. Gorman, E. G. Emiroglu, D. G. Hasko, and D. A. Williams, *Phys. Rev. Lett.* **95**, 090502 (2005).
⁶Y. Nakamura, C. D. Chen, and J. S. Tsai, *Phys. Rev. Lett.* **79**, 2328 (1997).
⁷T. Oosterkamp, T. Fujisawa, W. van der Weil, K. Ishibashi, R. Hijman, S. Tarucha, and L. Kouwenhoven, *Nature (London)* **395**, 873 (1998).
⁸J. R. Petta, A. C. Johnson, C. M. Marcus, M. P. Hanson, and A. C. Gossard, *Phys. Rev. Lett.* **93**, 186802 (2004).
⁹L. C. L. Hollenberg, A. S. Dzurak, C. Wellard, A. R. Hamilton, D. J. Reilly, G. J. Milburn, and R. G. Clark, *Phys. Rev. B* **69**, 113301 (2004).
¹⁰X. Hu and S. Das Sarma, *Phys. Rev. Lett.* **96**, 100501 (2006).
¹¹B. Kane, *Nature (London)* **393**, 133 (1998).
¹²L. C. L. Hollenberg, C. J. Wellard, C. I. Pakes, and A. G. Fowler, *Phys. Rev. B* **69**, 233301 (2004).
¹³M. J. Testolin, A. D. Greentree, C. J. Wellard, and L. C. L. Hollenberg, *Phys. Rev. B* **72**, 195325 (2005).
¹⁴A. J. Skinner, M. E. Davenport, and B. E. Kane, *Phys. Rev. Lett.* **90**, 087901 (2003).
¹⁵L. C. L. Hollenberg, A. D. Greentree, A. G. Fowler, and C. J. Wellard, *Phys. Rev. B* **74**, 045311 (2006).
¹⁶X. Hu, B. Koiller, and S. Das Sarma, *Phys. Rev. B* **71**, 235332 (2005).
¹⁷B. Koiller, X. Hu, and S. Das Sarma, *Phys. Rev. B* **73**, 045319 (2006).
¹⁸S. D. Barrett and T. M. Stace, *Phys. Rev. Lett.* **96**, 017405 (2006).
¹⁹A. Y. Smirnov, *Phys. Rev. B* **67**, 155104 (2003).
²⁰A. Y. Smirnov, *Phys. Rev. B* **68**, 134514 (2003).
²¹W. Kohn, in *Solid State Physics*, edited by F. Seitz and D. Turnbull (Academic, New York, 1957), Vol. 5.
²²L. A. Openov, *Phys. Rev. B* **70**, 233313 (2004).
²³M. Friesen, *Phys. Rev. Lett.* **94**, 186403 (2005).
²⁴C. W. Gardiner, *Quantum Noise* (Springer-Verlag, Berlin, 1991).
²⁵H. Carmichael, *An Open Systems Approach to Quantum Optics* (Springer-Verlag, Berlin, 1993).
²⁶R. Aguado and L. P. Kouwenhoven, *Phys. Rev. Lett.* **84**, 1986

- (2000).
- ²⁷R. Schoelkopf, A. Clerk, S. Girvin, K. Lehnert, and M. Devoret, cond-mat/0210247 (unpublished).
- ²⁸D. Jamieson *et al.*, Appl. Phys. Lett. **86**, 202101 (2005).
- ²⁹S. R. Schofield, N. J. Curson, M. Y. Simmons, F. J. Ruess, T. Hallam, L. Oberbeck, and R. G. Clark, Phys. Rev. Lett. **91**, 136104 (2003).
- ³⁰B. Koiller, X. Hu, and S. Das Sarma, Phys. Rev. Lett. **88**, 027903 (2002).